

Library

# Ball Retroreflector Optics

M.A. Goldman

March 23, 1996

## Abstract

The design and optical properties of ball retroreflectors are discussed. Ray tracing computations are given for the University of Arizona reflectors to be used at the GBT. Applications to the GBT are discussed.

## 1. Ball Reflector Design

Ball retroreflectors are back reflecting mirrors with a wide field angle of view. They are scheduled to be used as position indicating reference targets on the Green Bank Telescope. They will be mounted at several locations below the telescope's main reflector and on the feed arm. Electronic distance measuring laser scanners will find the distance from a characteristic fiducial reference point of the laser scanner to the center of curvature of the ball reflector. The construction, design, and behavior of these devices is discussed in this note.

Considered as an abstract geometric configuration, the ball retroreflector consists of two half balls of a uniform transparent optical medium, joined at their plane boundary disks so that the centers of curvature of the two half balls meet and identify to a common point. (Let us call this common point, which will be a center of curvature of each of the two hemispherical ball surfaces, the "center point" of the ball reflector. Let us call the common boundary plane of the half balls the "junction plane.") The half balls are optically non-absorbing and have the same index of refraction. The common intersection disk of the half balls is, then, not a surface of optical discontinuity. Such a configuration could in principle be fabricated by manufacturing two half balls and then joining them with an optical cement of matching index. In practice it is not easy to join two half balls precisely at their centers of curvature, and the configuration is fabricated differently. A full

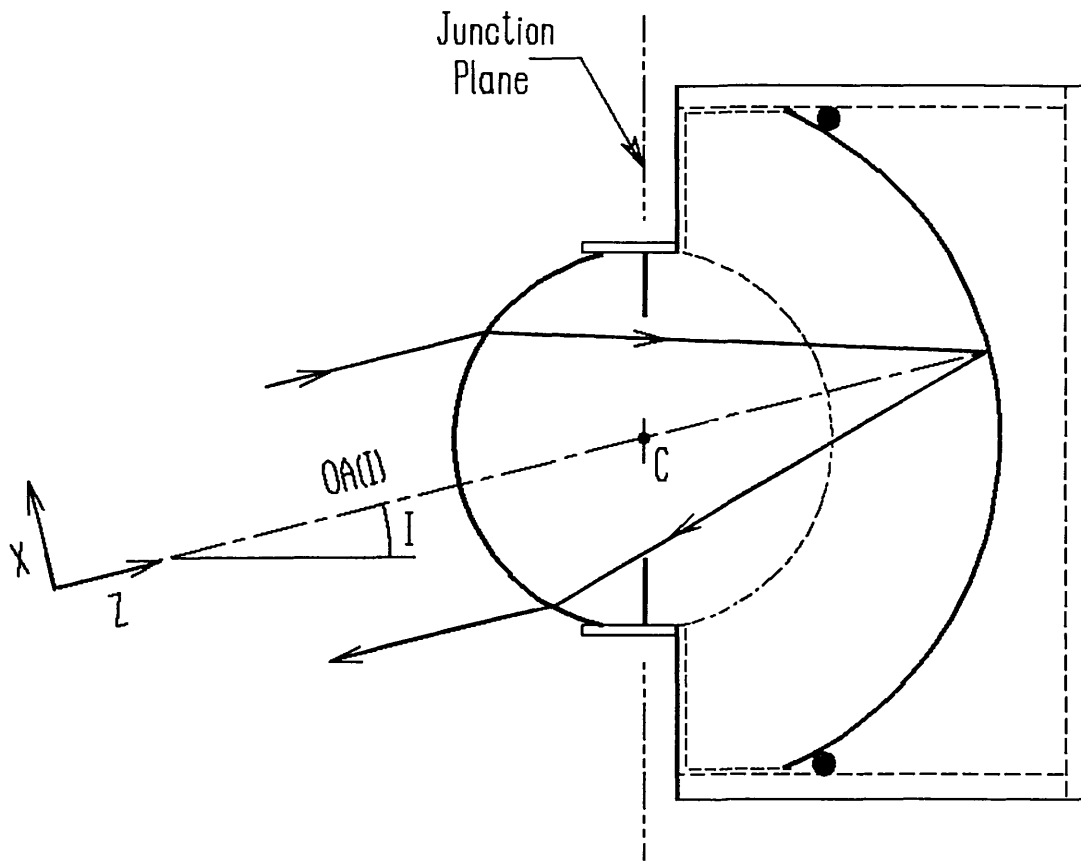


Figure 1. The Ball Retroreflector

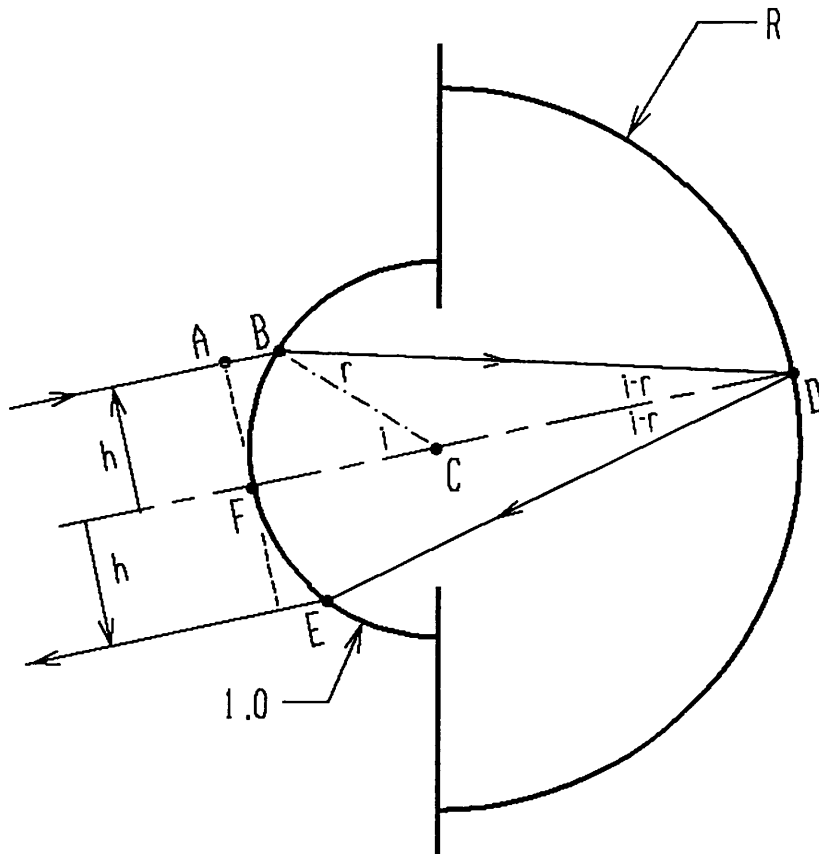


Figure 2. Ray Incidence For Correct Retroreflection

ball is made whose radius is that of the smaller half ball. A spherical ball cap shell is also fabricated. The outer radius of this cap is equal to the larger ball radius. The inner radius of the cap is slightly larger than that of the full ball so that when the small full ball and the annular cap are joined they fit together smoothly. It is easier to manufacture tooling to make a cap shell with accurately concentric hemisphere surfaces than it is to accurately join two half balls concentrically with a plane interface which is stable against shear stress damage. The full ball and the cap shell fit together without need for fixturing to maintain concentricity.

During fabrication, an annular rim and an annular groove are ground on the ball to generate a mounting surface and a stop aperture. The cap's outer ball surface is ground cylindrically to generate a mounting surface for the device; the cylinder axis is the normal line to the junction plane, through the reflector's center point. [Fig. 1].

The rear surface of the cap is given reflecting and protective coatings, to produce a reflecting rear spherical surface.

The configuration of two half balls is not a perfect retroreflector ideally, but in practice it is good and has the advantage of a wide acceptance angle range.

Let us examine the operation of this optical device.

To simplify the discussion we assume that the smaller radius of the front half ball is 1 and the larger rear ball radius is  $R$ . The results will depend only on the ratio of the two radii. We suppose that a collimated cylindrical light beam is incident on the reflector, not necessarily directed normal to the junction plane. We call a ray, which is normal to the front hemisphere at its point of entry (and is then undeflected on entry into the glass) and which also passes through the reflector center point, a "central ray." Such a ray will be normally incident on the rear hemisphere, because the two balls are concentric. The ray will return back on itself on reflection and will exit the small hemisphere normally, without deflection. The central ray then can be considered to be an "optical axis" of the incident collimated beam. The central ray will be perfectly retroreflected. When studying the stops and pupils of the reflector for collimated beams landing obliquely, with respect to the junction plane, we will specify them, in a given situation, as a function of the angle  $I$  between the axis in question  $OA(I)$  and the normal to the junction plane. When we perform ray trace computations, we will use local cartesian coordinates:  $X, Y, Z$ , where  $Z$  is along the local optic axis  $OA(I)$  and  $X$  and  $Y$  are transverse to this axis.

We now consider a ray parallel to the above-defined optical axis,  $OA(I)$ , at

normalized distance  $h$  from the axis. For this ray to retroreflect perfectly it must exit the reflector parallel to its entry direction, and at distance  $h$  from the axis. Furthermore, its forwards path (from point of entry to point of intersection with the rear hemisphere) will be a reflection of its backward path (from that point of intersection to the point of exit from the front hemisphere) about the axis, in the plane of the axis and incident ray. The ray will land on the rear hemisphere on the optical axis.

The angles of incidence and refraction are obtained easily from geometry and Snell's law. Call  $\eta = \eta_{glass}/\eta_{air}$ . Then:

$$\sin i = h, \quad \cos i = \sqrt{1 - h^2}, \quad \sin r = (\sin i)/\eta = h/\eta, \quad \cos r = (1/\eta)\sqrt{\eta^2 - h^2}.$$

In Fig. 2, applying the law of sines to triangle BCD,

$$R/1.0 = \sin r / \sin(i - r) = (h/\eta) \sin(i - r), \text{ giving}$$

$$\sin(i - r) = h/\eta R \quad \text{and} \quad \cos(i - r) = (1/\eta R) \sqrt{\eta^2 R^2 - h^2}. \text{ These give}$$

$$\tan(i - r) = \frac{h}{\sqrt{\eta^2 R^2 - h^2}} \quad \text{and} \quad h \cot(i - r) = \sqrt{\eta^2 R^2 - h^2}.$$

which is the projection of ray segment BD on the optical axis.

We then have  $h \cot(i - r) = R + \cos i$  giving an equation of restraint relating the quantities  $h$  and  $R$ :

$R + \sqrt{1 - h^2} = \sqrt{\eta^2 R^2 - h^2}$  which is solved to give  $R$  as a function of  $h$  and  $\eta$ ,

$$(1.1) \quad R = \frac{\sqrt{1-h^2} + \sqrt{\eta^2 - h^2}}{\eta^2 - 1}.$$

For a given value of  $R$ , only two axis-parallel rays give perfect retroreflection, one at  $h = 0$  and the other at the value of  $h$  satisfying the equation of constraint above. Actually, for any particular value of  $R$ , there will be a continuous range of  $h$ -values which give good retroreflection.

We tabulate below the ray height  $h$  for perfect retroreflection versus the ratio  $R$  of ball radii, using the index of refraction ratio  $\eta = 1.511186/1.000290 = 1.51075$  for BK7 glass in air, at wavelength  $\lambda = 0.78\mu\text{m}$ :

Axis-parallel ray height in units of entry ball radius.	Ratio of ball radii.
$h$	$R$
( $\rightarrow 0$ )	1.9579
0.2	1.9318
0.4	1.8508
0.6	1.7051
0.8	1.4673
0.9	1.2861
0.96	1.1280
0.98	1.0518

## 2. The University of Arizona Ball Retroreflectors

These units were designed by Roland V. Shack of the University of Arizona's Optical Sciences Center, Tucson, Arizona and 18 units are being manufactured for the Green Bank Telescope. under the direction of Martin J. Valente. They are made of Schott BK7 glass. The ball radii are  $R_1 = 1.969''$  and  $R_2 = 3.799''$ . The junction plane stop aperture diameter is  $0.906''$ . The ratio of radii is 1.92941, corresponding to perfect retroreflection of an axis-parallel ray with  $hR_1 = 0.20882 \times 1.969'' = 0.4112''$ .

A description of the reflectors is given in the retroreflector assembly drawings (NRAO): D35420M072, D35420A003, D35420A004 (February 17, 1995).

Ray trace simulations of the ball reflectors were made using the code BEAM THREE (Stellar Software, Berkeley CA).

Tracings of rays parallel to the optic axis  $OA(I)$  show that the slopes of the return rays relative to the optic axis are small when the ray distance from the

optic axis is less than the ray distance for perfect retroreflection,  $h$ . Rays more distant than  $h$  from the optic axis diverge rapidly with increasing displacement from the axis. This result is independent of the ray bundle orientation angle  $I$  to the junction plane normal. The slope of an exit ray leaving the reflector, with respect to the optic axis is nearly directly proportional to the landing height of the ray on the mirror surface, measured from the axis.

The field of view of oblique ray bundles is determined primarily by the ray stop aperture located at the junction plane rather than by the ball surfaces, which are concentric and spherically symmetric. It is interesting to compare the pupils of the reflector for the cases of normal and oblique ray bundle incidence with respect to the junction plane. At normal incidence the entrance and exit pupils of the reflector coincide; the stop aperture plane defines the junction plane and is perpendicular to the optical axis. The entrance pupil is found by imaging the stop through the front surface; for normal incidence the entrance pupil plane is the junction plane itself as a consequence of the stop plane's placement at the center of curvature of the front ball. The entrance pupil diameter  $D_{pe}$  is found by ray tracing a normal bundle through the reflector. It turns out to be  $D_{pe} = 1.338''$  for the Green Bank reflectors, when the finite stop thickness of  $0.118''$  is taken into account in the ray traces. (Ray traces made assuming a zero thickness stop at the junction plane gave an entrance pupil diameter of  $1.355''$ ).

The exit pupil is found by imaging the stop first through the rear mirror surface and then through the front ball surface. For normal incidence the junction plane is the paraxial image plane of unit magnification of the mirror surface, and the object for the second imaging is just the inverted stop aperture, which coincides with the stop aperture. For oblique incidence, the stop aperture plane is tilted with respect to the optical axis, and the stop's mirror image has opposite tilt. The pupil closes in one dimension and its shape changes from that of a circle to that of a "cat's eye."

Ray traces have been made for collimated ray bundles, that is sets of rays parallel to the optic axis  $OA(I)$ , for various angles of incidence  $I$ . These rays are generated, using a random number generator, to start uniformly-distributed over a square of side  $D_{pe}$ , the square being centered on the optic axis  $OA(I)$  and normal to it at the vertex of the first ball surface. Only rays at a distance  $\leq D_{pe}/2$  from  $OA(I)$  can pass through the retroreflector without blockage by the aperture stop. The fraction of rays incident at angle  $I$  and lying within a circular disk of diameter  $D_{pe}$  which pass through the reflector and return is compared to the fraction of rays entering normal to the junction plane and lying within the entrance pupil

Using the design values:  $R_1 = 1.969''$ ,  $R_2 = 3.799''$ , and group indexes  $\eta_{gG} = 1.527463$  for BK7 glass at  $0.78\mu\text{m}$ ,  $\eta_{gA} = 1.00025324$  for air at  $20^\circ\text{C}$ , 933mb pressure and 50% relative humidity, the length correction constant is nominally  $L_c = -173.715\text{mm} = -6.8392''$ . That is, the actual distance to the ball center point is the measured distance minus 173.715mm.

The correction  $L_c$  is independent of the angle  $I$  between the optic axis and the junction plane normal direction.

## 4. Discussion

### 4.1. Reflector Power Return

The ball retroreflectors have wide angle response, to  $\pm 65$  degrees of the junction plane normal. That is, they allow viewing within a cone of full angle 130 degrees, or  $0.577 \times 2\pi$  steradian. Ray trace simulations indicate that the return power response to a flat illumination field is insensitive to the illumination direction for incidence angles up to 40 degrees, for ranges between 60 and 200 meters, with an 80 mm detector aperture, and is considerable up to 65 degrees incidence. At larger incidence angles the return beam is vignetted by the outer rim of the reflector and the return drops sharply with increasing angle. This is easily confirmed by visually inspecting a reflector and changing the angle of view.

The effect of finite thickness of the reflector's junction plane stop is to reduce the entrance pupil diameter from 1.355" to 1.338" at normal incidence. The relative efficiency of reflection is not changed appreciably for view angles below 45 degrees; at larger view angles the effect of finite stop thickness is to decrease reflection efficiency. Curves of relative ray reflection versus view angle are given in Appendix A for the cases of assumed zero and finite thickness stopping.

The range length correction  $L_c$  is a constant for each ball reflector, and is independent of range and incidence angle (unlike glass cube corners). For each milli-inch increase of outer ball radius from the design radius the length correction constant increases by 1.5 milli-inches in amplitude; for each milli-inch increase of front ball radius from the design radius the length correction constant increases by 0.5 milli-inches in amplitude. The tolerances on the ball radii in manufacture are  $\pm 1$  milli-inch. Each ball reflector may have to be individually calibrated for range length correction. If, in manufacture, the diameter of the front ball before assembly and the sum of the ball radii (that is the total glass thickness) after assembly could be measured to 0.5 milli-inch, for example with a spherometer,

*Please insert the attached page 6 to GBT Memo #148 titled, "Ball Retroreflectors Optics", by Michael Goldman dated March 23, 1996.*

*Library*



disk, to estimate relative power reflection as a function of incidence angle at, close range. The ray traces then follow the path of the exit rays from the reflector to their landing on test surfaces at 40, 60, 100, 120 and 200 meter distances from the reflector center, to display the divergence of the exit rays from the reflector. It was found that the reflected ray bundle is composed of two components, a slowly diverging well-defined "core" surrounded by a more rapidly diverging cloud .

The ray traces were repeated with an additional constraint: a stop aperture 3.15" diameter was placed just before the landing plane to define those rays which can enter the detector lens of a GBT laser scan unit at the test surface. The fraction of rays which pass through the detector lens aperture, relative to the rays which pass through the entrance pupil at normal incidence was found, as the angle of incidence  $I$  was varied.

At distances of 60, 120 and 200 meters the angular response appears essentially flat for incidence angles between 0 and 40 degrees, and decreases gradually for angles up to 65 degrees. It was found observationally by D. Bradley that beyond 66 degrees incidence the first ball rim starts to vignette the rays and the response decreases rapidly thereafter [D. Bradley, GBT Document Archive memo L0082, March 1996]. Numerical and graphical results of the tracings are given in Appendix A.

### 3. The Length Correction Constant

When the ball reflector is used as part of an electronic distance measuring system, the round trip propagation time delay through the reflector will be equal to twice the sum of the ball radii divided by the group propagation velocity:  $\Delta t_{glass} = 2(R_1 + R_2) / (c_o \eta_{gG})$ . One wishes to measure the distance in air between a distant reference point and the ball center which lies on the propagation path. The round trip propagation time for a light signal in air to travel a distance of two front ball radii is  $\Delta t_{air} = 2R_1 / (c_o \eta_{gA})$ . The excess propagation time  $(\Delta t_{glass} - \Delta t_{air})/2$  appears as an excess length of air path  $\{(\eta_{gG}/\eta_{gA})(R_1 + R_2) - R_1\}$  which must be subtracted from the measured equivalent air path. The distance:

$$(3.1) \quad L_c = (-1) \{(\eta_{gG}/\eta_{gA})(R_1 + R_2) - R_1\}$$

is a length correction which must be added to the measured air equivalent path to measure to the center of the retroreflector. The correction  $L_c$  is the "prism constant" for this glass retroreflector, and is analogous to the "prism constant" correction used for glass cube corner retroreflectors in commercial electronic distance measurement systems.



this could avoid the need for individual calibrations. Also, it would be desirable to have a fiducial reference flat area on the ball mount housing at a standard distance or at least a known distance from the junction plane (which passes through the common ball center point) and parallel to the junction plane.

When illuminated by a laser range scanner, the return from a ball reflector depends upon: the illuminating laser's beam-width profile at the ball, the angle of incidence to the ball's junction plane normal, the return range to the laser scanner, and the diameter of the scanner's detector lens. The gaussian beam diameter of the  $0.78\mu\text{m}$  wavelength beam from a model LT 021 MD diode laser (Melles-Griot, product series number 56 DLB 305) is close to one inch at 120 meters range and is about 3.2 inches at 200 meter range. The illuminating beam's profile is well matched to the entrance pupil of the ball reflector for ranges to 120 meters, and strong return is expected at these ranges. At 200 meter range between scanner and ball reflector, about 10% of the incident beam power will be incident on the ball, because of the spreading of the laser beam. An additional ball return loss of 11 to 15dB is expected, which depends upon the incidence angle. The total propagation loss at 200m range is expected to be 21 to 25dB. Laser scanners have operated dynamically under field conditions, including atmospheric refraction effects, with 27dB return loss. The slant range of a laser beam from a ground station 120 meters away from the telescope's center bearing to the top of the feed arm at maximum height is a little less than 200 meters. It appears that the ball reflectors should have sufficient power return to be useful over the distance ranges and incidence angles required for the GBT.

#### 4.2. Reflector Deployment

The ball retroreflector has the following properties: it has wide angle response, is polarization insensitive, and its length correction is independent of viewing angle. Its response is also independent of the roll direction of the incident radiation about the about the junction plane normal. The light entering a ball reflector essentially is always normally incident on the rear mirror surface, and the reflected radiation has the same polarization orientation as the incident radiation, even though the rear mirror surface is metal coated. The ball reflector is appreciably more expensive than cube corner reflectors.

When considered as a candidate for deployment in the Green Bank Telescope's laser metrology system, it should be compared to competing retroreflectors: the hollow metal, and uncoated and metal-coated glass prism cube corners.

The unmetallized glass reflector is inexpensive, polarization sensitive, has roll-orientation-sensitive return which mixes polarizations, and has an incidence-angle-dependent length correction and narrow angle response. Typically these reflectors are used when incidence is within ten degrees of the entry surface normal. The glass prism retroreflector has been analyzed by Peck [E.R. Peck, J.O.S.A. 38, 1015(1948) , *ibid* 52, 253(1961)], Eckhardt [H.D. Eckhardt, Applied Optics 10, 1559(1971)], and Player [M.A. Player, J. Modern Optics 35, 1813(1988)].

The glass reflector with metal coating on the three reflecting surfaces is less polarization and roll sensitive. It also has incidence-angle-dependent length correction. The metal coating must be protected against mechanical abrasion, corrosion, and weather damage. Some cross-polarization appears after triple reflection, but not as severely as for the uncoated prism. The angular field of view is broad. The optical properties of metal coated glass cube corner prisms have been studied by Hege and Leonhardt [G. Hege and K. Leonhardt , Optik 47, 167(1977)], Leonhardt and Burckhardt [K. Leonhardt and C. Burckhardt, Optik 47, 215(1977)], and Kothiyal [M.P. Kothiyal, Optik 62, 199(1982)].

The hollow metal corner requires no length correction. A reference point exists at the intersection of the three reflecting surface planes. A plane wave will retroreflect from a virtual plane normal to the direction of incidence, and the virtual plane will pass through this reference point. There is some cross-polarization due to oblique reflections at the three corner faces. The angular response of the hollow corner is limited by the requirement that the incident radiation reflect from all three faces. The maximum angle of incidence is roll-angle-dependent. It has been studied by Rityn [N.E. Rityn, Sov. J. Opt. Tech. 34. 198(1967)]. The maximum angle of incidence varies from approximately 32 to 57 degrees from the cube body-diagonal direction, depending upon the roll of the plane of incidence (defined by the incoming ray and the body diagonal) with respect to the corner edges.

In the Green Bank Telescope's laser metrology system retroreflectors may be employed in a variety of situations. They can be ground-based at fixed locations, to serve as survey control reference points. They may be employed aloft, to serve as sighting reference points on rigid or flexible structural members of the telescope. They can be used as fiducial locating references in static structural inspections. They can be used as instantaneous range location fiducials during dynamical laser range determinations. They may be ground-based, and scanned by fixed ground-based lasers or by moving feed arm based lasers. They may be on or below the

telescope main reflector, on the feed arm, on the secondary reflector or other moving telescope member and be scanned by ground-based or telescope-based lasers. They may be used for main reflector dish shaping , telescope pointing or structural deflection determinations.

The appropriate type of reflector to be used in any of these distinct situations will depend on the number of lasers that will have to scan the reflector, the range of laser scan azimuth and elevation angles required for each type of measurement, and the range of reflector illumination incidence and roll angles needed during each dynamical laser scan.

The ball reflector will be effective where wide angle viewing is needed, either by a single laser scanner in a dynamical measurement, or during simultaneous viewing by many scanners during a range determination. Freedom from polarization effects, and roll-independent maximum viewing angle will improve the reliability of scan measurements. Finally, the independence of the length correction upon range distance and illumination incidence angle means that dynamically-updated software length corrections will not be required during dynamical ranging measurements.

## Appendix A

### Ray Transmission Through The Ball Retroreflector

Random ray traces were run for collimated ray bundles incident on the ball retroreflector.

A collimated ray bundle is incident on the reflector at an angle  $I$  to the normal direction to the junction plane, which is the aperture stop plane. The stop center is the common ball center point. A single ray on the bundle is distinguished by the property that it passes through the ball center point. This ray is perpendicular to the ball surfaces at entry and exit, and is deviated by a back reflection onto itself at the mirror surface, but is not deviated at the first ball surface on entry or exit. The ray then acts as an optical axis,  $OA(I)$ , for the bundle of parallel rays incident at angle  $I$ .

The following  $(X,Y,Z)$  coordinate system is used in the ray traces:

The origin of coordinates is at the common ball center.

$X$  is the transverse coordinate, in the plane of incidence, of a ray point, with respect to  $OA(I)$ ,

$Y$  is the transverse coordinate, perpendicular to the plane of incidence, of a ray point,

$Z$  is the axial coordinate of a ray point, along the optic axis  $OA(I)$ .

The landing point of a ray on the  $i$ 'th optical surface of the system is  $(X_i, Y_i, Z_i)$ . A ray propagates from the source plane  $X_0, Y_0$  from a source point  $(X_0, Y_0, Z_0)$ .

The stop aperture in the ball reflector is of finite thickness, 0.118". The aperture is specified to have a rounded internal rim, that is a toric rim surface, in a vendor drawing of the reflector. The manufactured ball retroreflector was observed to have a cylindrical rim surface. To study the effect of stop thickness, two models of the stop were examined. The first model assumed a single iris, of zero thickness. The second model used three parallel iris apertures, spaced at 0.059" from one another; the middle iris was at the common ball center.

By carrying out repeated ray traces at normal incidence to the junction plane ( $I = 0$ ) it was found that the largest collimated ray bundle to pass through the aperture was of diameter 1.355 inches for the single thin aperture model and 1.338" for the finite thickness (three aperture) stop model.

A ray source file, RETBALLQ.RAY, was prepared listing 20 rays parallel to the Z axis which were at or within 1.338" from the axis. When the "random" option of the BEAM THREE code is selected (using a source file for a collimated bundle) it generates, using a random number generator, a sequence of rays which are uniformly distributed over the range of transverse X and Y coordinates spanned in the  $X_0, Y_0$  source plane. When "random" rays are traced for this ray source file, axis-parallel rays are generated which uniformly fill a 1.338" square centered on the Z axis, which is the optical axis  $OA(I)$ . A fraction  $\pi/4$  of these rays pass through the reflector, just those rays which enter within a circular entrance pupil disk of diameter 1.338" =  $D_{pe}$ .

Ray traces were carried out to find the fraction of rays entering the 1.338" circular entrance pupil disk uniformly distributed over the pupil area, which are retro-reflected and land within an optical-axis-centered circular aperture of 3.15" diameter (80.0mm), at various distances from the reflector. This is the acceptance aperture of the GBT laser scanner detector lens.

The fractional transission is equal to the ratio of finish rays multiplied by  $(4/\pi)$ , to the number of start rays (uniformly distributed over an axis-centered 1.338" square). The sample standard error of the number of finish rays is approximately equal to the square root of the number of finish rays.

This statistical ray modeling procedure was also carred out for the thin stop model, using the larger entrance pupil diameter.

Axis-Parallel Ray Transmission Through The  
Ball Retroreflector And Scanner Lens Aperture

Ray starts are through a 1.3376" square aperture centered on the optic axis (Z axis), at the first ball surface vertex; sides of the square are parallel to the local X,Y axes. Axis-parallel rays are generated, using a random number generator, distributed uniformly over the square. The entrance pupil of the iris at normal incidence is a circular disk of diameter 1.3376 inches. Three irises are used to model the 0.118" thick ball stop aperture.

INCIDENCE ANGLE ( I ) [Degrees]	FRONT VERTEX PLANE [Z=-1.969"]	Exit ray finishes at front ball vertex plane, after ray entry into the reflector and back reflection through the glass.	
	Starts	Finishes	$(4/\pi) \cdot (\text{Finishes}/\text{Starts})$
0	40296	31663	1.0005
5	19400	14777	0.9698
10	15387	11127	0.9207
15	14636	10247	0.8914
20	15560	10246	0.8384
25	16808	10309	0.7803
30	17300	9932	0.7310
35	19100	10120	0.6746
40	20300	9661	0.6060
45	22270	9303	0.5319
50	25000	9237	0.4704
55	29100	9042	0.3956
60	36300	8988	0.3153
63	41349	8895	0.2739
65	40512	7817	0.2457

INCIDENCE ANGLE ( I ) [Degrees]      RAY LANDING PLANE [Z=-60m]      Finishes through 3.15" diameter circular aperture (80.0mm aperture) at landing plane.

	Starts	Finishes	$(4/\pi) \cdot (\text{Finishes}/\text{Starts})$
0	61306	13526	0.2809
5	61500	13605	0.2817
10	62866	13846	0.2804
15	62776	13747	0.2788
20	61006	13340	0.2784
25	60287	13200	0.2788
30	60452	13206	0.2781
35	60270	13100	0.2767
40	60493	12186	0.2565
45	60710	10134	0.2125
50	61300	7980	0.1658
55	61837	6421	0.1322
60	64500	5528	0.1091
63	60300	4602	0.0972
65	70080	4942	0.0898

INCIDENCE ANGLE ( I ) [Degrees]      RAY LANDING PLANE [Z=-120m]      Finishes through 3.15" diameter circular aperture (80.0mm aperture) at landing plane.

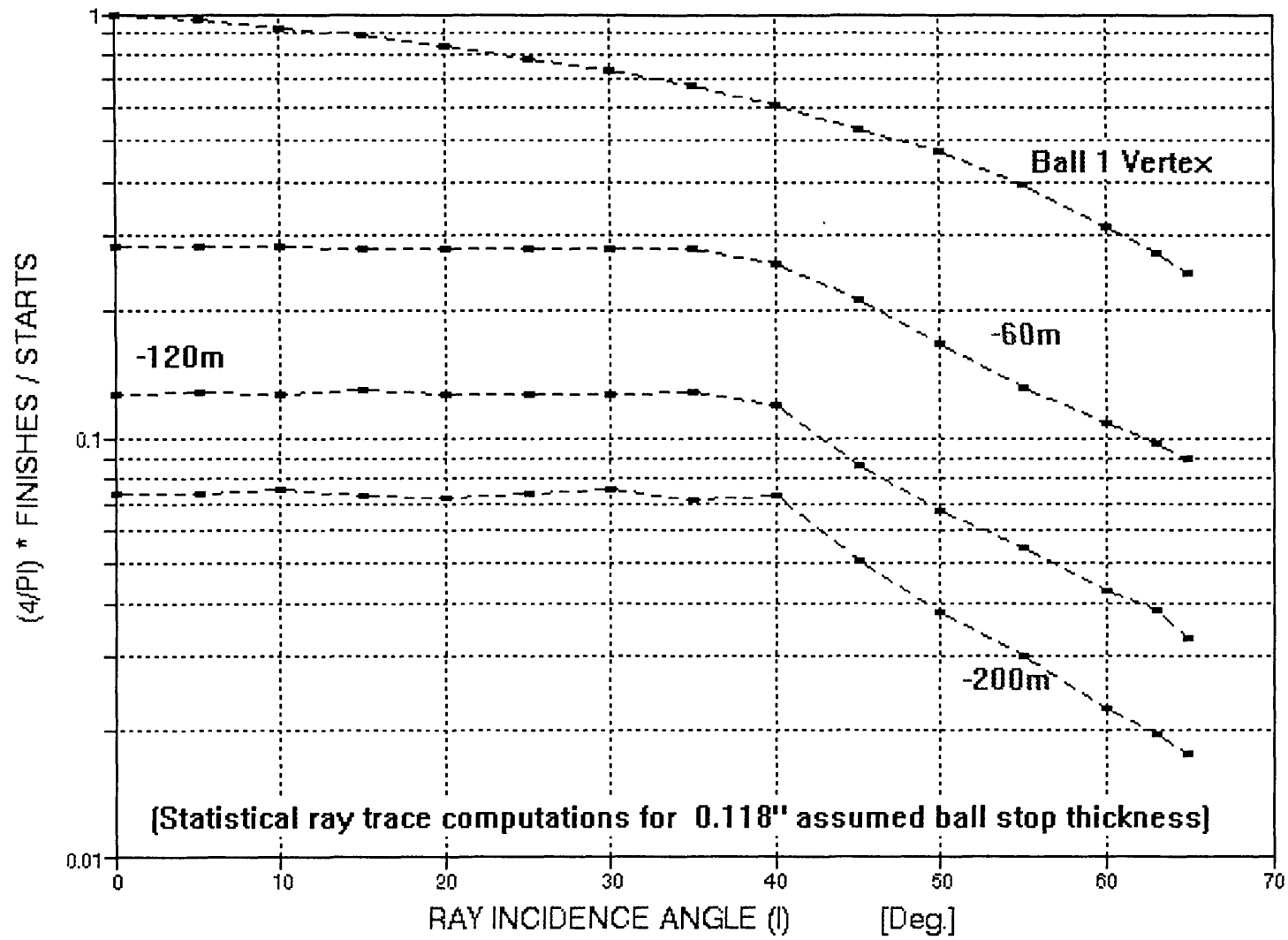
	Starts	Finishes	$(4/\pi) \cdot (\text{Finishes}/\text{Starts})$
0	99310	9847	0.1263
5	65856	6630	0.1282
10	64100	6333	0.1256
15	63000	6372	0.1288

20	62666	6170	0.1254
25	61700	6144	0.1268
30	61007	6039	0.1260
35	54200	5431	0.1276
40	65488	6112	0.1189
45	59600	4055	0.0866
50	76152	3982	0.0666
55	81600	3499	0.0546
60	60400	2670	0.0429
63	80300	2415	0.0383
65	81491	2121	0.0331

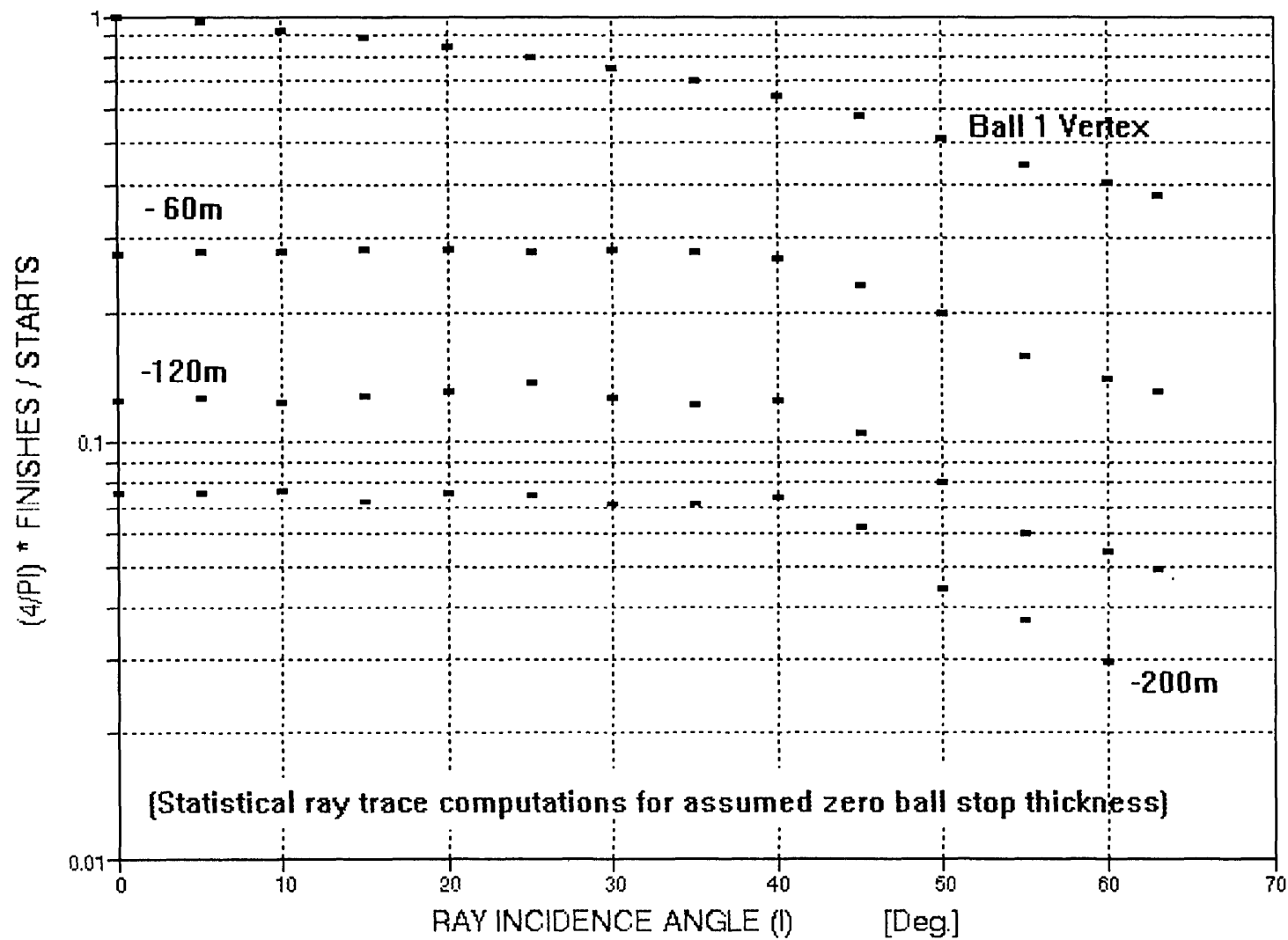
INCIDENCE ANGLE ( I ) [Degrees]      RAY LANDING PLANE [Z=-200m]      Finishes through 3.15" diameter circular aperture (80.0mm aperture) at landing plane.

	Starts	Finishes	$(4/\pi) \cdot (\text{Finishes}/\text{Starts})$
0	100269	5814	0.0738
5	38246	2205	0.0734
10	36000	2122	0.0751
15	35949	2066	0.0732
20	35647	2016	0.0720
25	35428	2051	0.0737
30	34497	2043	0.0754
35	36652	2034	0.0707
40	32169	1826	0.0723
45	46100	1849	0.0511
50	54950	1646	0.0381
55	68263	1609	0.0300
60	88601	1572	0.0226
65	100700	1381	0.0175

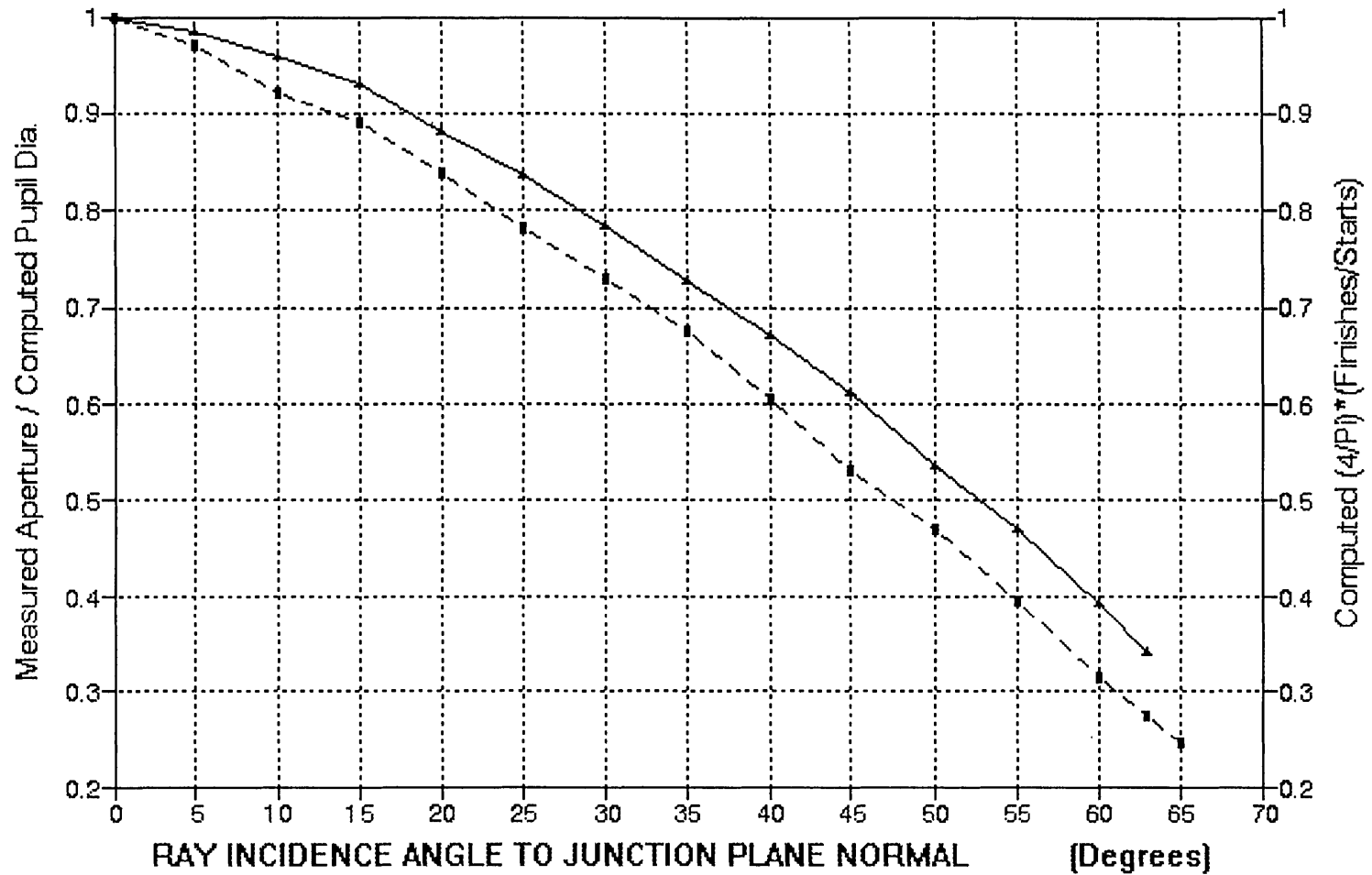
# RELATIVE RAY TRANSMISSION THROUGH BALL REFLECTOR AND SCANNER LENS STOP



# RELATIVE RAY TRANSMISSION THROUGH BALL REFLECTOR AND SCANNER LENS STOP



# BALL RETROREFLECTOR APERTURE VERSUS ILLUMINATION INCIDENCE ANGLE



Measured (D. Bradley) ▲

Statistical Ray Traces To Ball Vertex Plane, -■- Assuming 0.118" Stop Width

7 surfaces RETBALL1.OPT March 19, 1996

Index	Zvertex	Curvature	Mir/Lens	Diameter	Notes
1.00029	-1.969	0.0			:#1, Reference Plane
1.0029	-1.969	0.507872	Lens	3.938	:#2, Ball 1, Entry
1.511186	0.00	0.0	iris	0.906	:#3, Stop Plane
1.511186	3.799	-0.2632271	Mirror	7.598	:#4, Ball 2, Mirror
1.511186	0.0	0.0	iris	0.906	:#5, Iris, Return
1.511186	-1.969	0.507872	Lens	3.938	:#6, Ball 1, Return
1.00029	-1.969	0.0			:#7, Reference Plane
[Entry	:	(At Vertex):	:	:	:
Medium]	[Inches]	[1/Inches]:	:	[Inches]:	:

This file contains optical surface data used for a (BEAM THREE code) ray trace simulation of the University of Arizona ball retro-reflectors manufactured for the NRAO Green Bank Telescope. The glass index used is the phase index for BK7 glass, at 0.78um wavelength. The ratio of the ball radii is 3.799"/1.969" = 1.929406.

The stop aperture of the ball is assumed to be of zero thickness in ray traces made using this file.

17 rays RETBALL1.RAY March 19, 1996

X0	Y0	Z0	U0	V0	W0	X4	X7	W7
0.05	0.0	- 1.969	0.0	0.0	1.0			
0.15	0.0	- 1.969	0.0	0.0	1.0			
0.25	0.0	- 1.969	0.0	0.0	1.0			
0.35	0.0	- 1.969	0.0	0.0	1.0			
0.45	0.0	- 1.969	0.0	0.0	1.0			
0.55	0.0	- 1.969	0.0	0.0	1.0			
0.60	0.0	- 1.969	0.0	0.0	1.0			
0.668	0.0	- 1.969	0.0	0.0	1.0			
0.6688	0.0	- 1.969	0.0	0.0	1.0			
0.6689	0.0	- 1.969	0.0	0.0	1.0			
0.669	0.0	- 1.969	0.0	0.0	1.0			
0.677	0.0	- 1.969	0.0	0.0	1.0			
0.6775	0.0	- 1.969	0.0	0.0	1.0			
0.6777	0.0	- 1.969	0.0	0.0	1.0			
0.678	0.0	- 1.969	0.0	0.0	1.0			
0.679	0.0	- 1.969	0.0	0.0	1.0			
0.680	0.0	- 1.969	0.0	0.0	1.0			

This file contains input ray data used for a (BEAM THREE code) ray trace simulation of the University of Arizona cat's eye retroreflector for the NRAO Green Bank Telescope.

Axis-parallel rays are incident at reference surface #0, tangent to the small hemisphere, perpendicular to the junction plane. Distances are in inches.

17 rays RETBALL1.Z March 19, 1996

X0	Y0	Z0	U0	V0	W0	X4	X7	W7
0.05	0.0	-1.969	0.0	0.0	1.0	0.0007	-0.05075	-1.0000
0.15	0.0	-1.969	0.0	0.0	1.0	0.0020	-0.15209	-1.0000
0.25	0.0	-1.969	0.0	0.0	1.0	0.0028	-0.25290	-1.0000
0.35	0.0	-1.969	0.0	0.0	1.0	0.0027	-0.35281	-1.0000
0.45	0.0	-1.969	0.0	0.0	1.0	0.0014	-0.45143	-1.0000
0.55	0.0	-1.969	0.0	0.0	1.0	-0.0016	-0.54832	-1.0000
0.60	0.0	-1.969	0.0	0.0	1.0	-0.0038	-0.59596	-1.0000
0.668	0.0	-1.969	0.0	0.0	1.0	-0.0079	-0.65974	-1.0000
0.6688	0.0	-1.969	0.0	0.0	1.0	-0.0079	-0.66048	-1.0000
0.6689	0.0	-1.969	0.0	0.0	1.0	-0.0079	-0.66057	-1.0000
0.669	0.0	-1.969	0.0	0.0	1.0	-0.0079	-0.66067	-1.0000
0.677	0.0	-1.969	0.0	0.0	1.0	-0.0085	-0.66808	-1.0000
0.6775	0.0	-1.969	0.0	0.0	1.0	-0.0085	-0.66854	-1.0000
0.6777	0.0	-1.969	0.0	0.0	1.0	:	:	:
0.678	0.0	-1.969	0.0	0.0	1.0	:	:	:
0.679	0.0	-1.969	0.0	0.0	1.0	:	:	:
0.680	0.0	-1.969	0.0	0.0	1.0	:	:	:

The last four rays are stopped.

X	Y	Z	U	V	W
0.050000	0.000000	-1.969000	0.000000	0.000000	1.000000
0.050000	0.000000	-1.969000	0.000000	0.000000	1.000000
0.050000	0.000000	-1.968365	-0.008543	0.000000	0.999964
0.033184	0.000000	0.000000	-0.008543	0.000000	0.999964
0.000728	0.000000	3.799000	-0.008926	0.000000	-0.999960
-0.033184	0.000000	-0.000000	-0.008926	0.000000	-0.999960
-0.050754	0.000000	-1.968346	-0.000317	0.000000	-1.000000
-0.050755	0.000000	-1.969000	-0.000317	0.000000	-1.000000
optical path =		17.43304979 inches			

X	Y	Z	U	V	W
0.150000	0.000000	-1.969000	0.000000	0.000000	1.000000
0.150000	0.000000	-1.969000	0.000000	0.000000	1.000000
0.150000	0.000000	-1.963278	-0.025673	0.000000	0.999670
0.099580	0.000000	0.000000	-0.025673	0.000000	0.999670
0.002017	0.000000	3.798999	-0.026734	0.000000	-0.999643
-0.099583	0.000000	-0.000000	-0.026734	0.000000	-0.999643
-0.152085	0.000000	-1.963118	-0.000863	0.000000	-1.000000
-0.152090	0.000000	-1.969000	-0.000863	0.000000	-1.000000
optical path =		17.43311105			

X	Y	Z	U	V	W
0.250000	0.000000	-1.969000	0.000000	0.000000	1.000000
0.250000	0.000000	-1.969000	0.000000	0.000000	1.000000
0.250000	0.000000	-1.953065	-0.042936	0.000000	0.999078
0.166066	0.000000	0.000000	-0.042936	0.000000	0.999078
0.002802	0.000000	3.798999	-0.044409	0.000000	-0.999013
-0.166077	0.000000	0.000000	-0.044409	0.000000	-0.999013
-0.252880	0.000000	-1.952694	-0.001141	0.000000	-0.999999
-0.252899	0.000000	-1.969000	-0.001141	0.000000	-0.999999
optical path =		17.43321507			

X	Y	Z	U	V	W
0.350000	0.000000	-1.969000	0.000000	0.000000	1.000000
0.350000	0.000000	-1.969000	0.000000	0.000000	1.000000
0.350000	0.000000	-1.937643	-0.060425	0.000000	0.998173
0.232703	0.000000	0.000000	-0.060425	0.000000	0.998173
0.002727	0.000000	3.798999	-0.061858	0.000000	-0.998085
-0.232724	0.000000	0.000000	-0.061858	0.000000	-0.998085
-0.352782	0.000000	-1.937139	-0.000964	0.000000	-1.000000
-0.352812	0.000000	-1.969000	-0.000965	0.000000	-1.000000

optical path = 17.43332489

X	Y	Z	U	V	W
0.450000	0.000000	-1.969000	0.000000	0.000000	1.000000
0.450000	0.000000	-1.969000	0.000000	0.000000	1.000000
0.450000	0.000000	-1.916888	-0.078240	0.000000	0.996935
0.299561	0.000000	-0.000000	-0.078240	0.000000	0.996935
0.001413	0.000000	3.799000	-0.078982	0.000000	-0.996876
-0.299579	0.000000	-0.000000	-0.078982	0.000000	-0.996876
-0.451426	0.000000	-1.916553	-0.000131	0.000000	-1.000000
-0.451433	0.000000	-1.969000	-0.000131	0.000000	-1.000000

optical path = 17.43338532

X	Y	Z	U	V	W
0.550000	0.000000	-1.969000	0.000000	0.000000	1.000000
0.550000	0.000000	-1.969000	0.000000	0.000000	1.000000
0.550000	0.000000	-1.890625	-0.096490	0.000000	0.995334
0.366719	0.000000	-0.000000	-0.096490	0.000000	0.995334
0.001563	0.000000	3.799000	-0.095670	0.000000	-0.995413
-0.366690	0.000000	0.000000	-0.095670	0.000000	-0.995413
-0.548444	0.000000	-1.891077	0.001582	0.000000	-0.999999
-0.548320	0.000000	-1.969000	0.001583	0.000000	-0.999999

optical path = 17.43332338

X	Y	Z	U	V	W
0.600000	0.000000	-1.969000	0.000000	0.000000	1.000000
0.600000	0.000000	-1.969000	0.000000	0.000000	1.000000
0.600000	0.000000	-1.875356	-0.105815	0.000000	0.994386
0.400439	0.000000	0.000000	-0.105815	0.000000	0.994386
-0.003822	0.000000	3.798998	-0.103814	0.000000	-0.994597
-0.400354	0.000000	-0.000000	-0.103814	0.000000	-0.994597
-0.596225	0.000000	-1.876560	0.002847	0.000000	-0.999996
-0.595962	0.000000	-1.969000	0.002848	0.000000	-0.999996

optical path = 17.43321909

X	Y	Z	U	V	W
0.668000	0.000000	-1.969000	0.000000	0.000000	1.000000
0.668000	0.000000	-1.969000	0.000000	0.000000	1.000000
0.668000	0.000000	-1.852225	-0.118751	0.000000	0.992924
0.446478	0.000000	0.000000	-0.118751	0.000000	0.992924
-0.007873	0.000000	3.798992	-0.114635	0.000000	-0.993408
-0.446261	0.000000	-0.000000	-0.114635	0.000000	-0.993408
-0.660318	0.000000	-1.854978	0.005086	0.000000	-0.999987
-0.659738	0.000000	-1.969000	0.005087	0.000000	-0.999987

optical path = 17.43296968

X	Y	Z	U	V	W
0.668800	0.000000	-1.969000	0.000000	0.000000	1.000000
0.668800	0.000000	-1.969000	0.000000	0.000000	1.000000
0.668800	0.000000	-1.851936	-0.118906	0.000000	0.992906
0.447021	0.000000	0.000000	-0.118906	0.000000	0.992906
-0.007928	0.000000	3.798992	-0.114761	0.000000	-0.993393
-0.446802	0.000000	0.000000	-0.114761	0.000000	-0.993393
-0.661065	0.000000	-1.854711	0.005116	0.000000	-0.999987
-0.660480	0.000000	-1.969000	0.005117	0.000000	-0.999987
optical path = 17.43296589					

X	Y	Z	U	V	W
0.668900	0.000000	-1.969000	0.000000	0.000000	1.000000
0.668900	0.000000	-1.969000	0.000000	0.000000	1.000000
0.668900	0.000000	-1.851900	-0.118925	0.000000	0.992903
0.447089	0.000000	-0.000000	-0.118925	0.000000	0.992903
-0.007935	0.000000	3.798992	-0.114776	0.000000	-0.993391
-0.446869	0.000000	-0.000000	-0.114776	0.000000	-0.993391
-0.661158	0.000000	-1.854678	0.005120	0.000000	-0.999987
-0.660573	0.000000	-1.969000	0.005121	0.000000	-0.999987
optical path = 17.43296541					

X	Y	Z	U	V	W
0.669000	0.000000	-1.969000	0.000000	0.000000	1.000000
0.669000	0.000000	-1.969000	0.000000	0.000000	1.000000
0.669000	0.000000	-1.851864	-0.118944	0.000000	0.992901
0.447157	0.000000	0.000000	-0.118944	0.000000	0.992901
-0.007941	0.000000	3.798992	-0.114792	0.000000	-0.993390
-0.446937	0.000000	0.000000	-0.114792	0.000000	-0.993390
-0.661252	0.000000	-1.854645	0.005124	0.000000	-0.999987
-0.660666	0.000000	-1.969000	0.005125	0.000000	-0.999987
optical path = 17.43296494					

X	Y	Z	U	V	W
0.677000	0.000000	-1.969000	0.000000	0.000000	1.000000
0.677000	0.000000	-1.969000	0.000000	0.000000	1.000000
0.677000	0.000000	-1.848954	-0.120488	0.000000	0.992715
0.452589	0.000000	0.000000	-0.120488	0.000000	0.992715
-0.008502	0.000000	3.798990	-0.116043	0.000000	-0.993244
-0.452348	0.000000	0.000000	-0.116043	0.000000	-0.993244
-0.668718	0.000000	-1.851966	0.005431	0.000000	-0.999985
-0.668082	0.000000	-1.969000	0.005433	0.000000	-0.999985
optical path = 17.43292579					

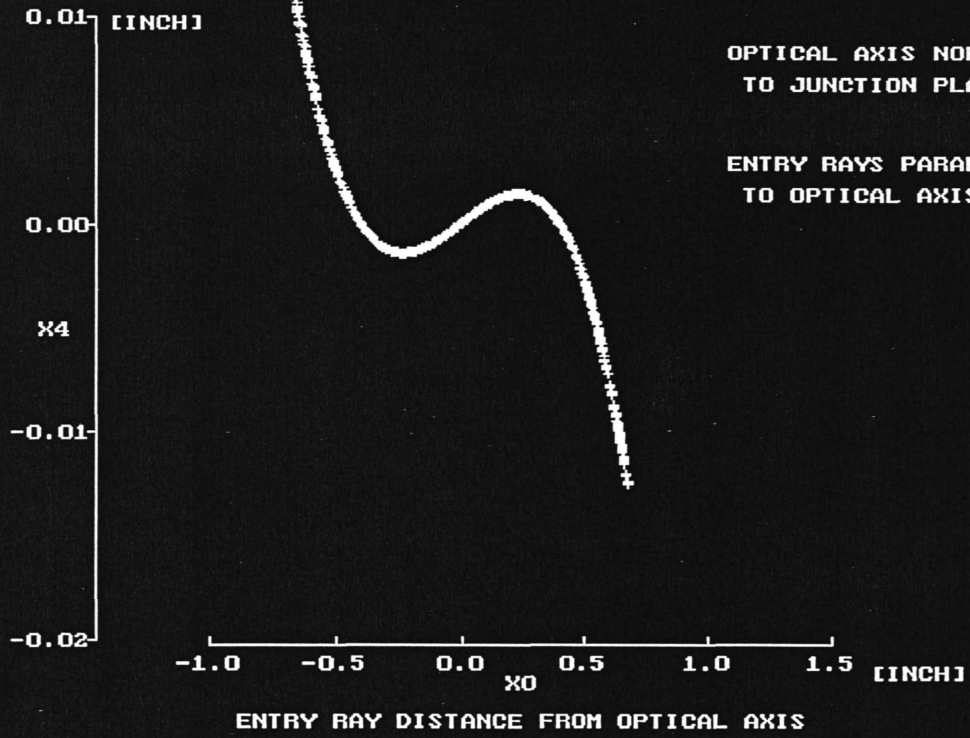
X	Y	Z	U	V	W
0.677500	0.000000	-1.969000	0.000000	0.000000	1.000000
0.677500	0.000000	-1.969000	0.000000	0.000000	1.000000
0.677500	0.000000	-1.848771	-0.120584	0.000000	0.992703
0.452928	0.000000	-0.000000	-0.120584	0.000000	0.992703
-0.008537	0.000000	3.798990	-0.116121	0.000000	-0.993235
-0.452686	0.000000	0.000000	-0.116121	0.000000	-0.993235
-0.669184	0.000000	-1.851798	0.005451	0.000000	-0.999985
-0.668545	0.000000	-1.969000	0.005453	0.000000	-0.999985
optical path = 17.43292327					

X	Y	Z	U	V	W
0.677700	0.000000	-1.969000	0.000000	0.000000	1.000000
0.677700	0.000000	-1.969000	0.000000	0.000000	1.000000

0.677700	0.000000	-1.848698	-0.120623	0.000000	0.992698
0.453064	0.000000	-0.000000	-0.120623	0.000000	0.992698
optical path =		2.93492607			

X	Y	Z	U	V	W
0.678000	0.000000	-1.969000	0.000000	0.000000	1.000000
0.678000	0.000000	-1.969000	0.000000	0.000000	1.000000
0.678000	0.000000	-1.848588	-0.120681	0.000000	0.992691
0.453268	0.000000	-0.000000	-0.120681	0.000000	0.992691
optical path =		2.93488892	inches		

RAY LANDING HEIGHT  
ON MIRROR SURFACE



X-AXIS DIRECTION COSINE  
OF EXIT RAY

0.008  
0.004  
U7  
0.000  
-0.004

0.0 0.4 0.8 [INCH]  
X0

ENTRY RAY DISTANCE FROM OPTICAL AXIS

OPTICAL AXIS NORMAL  
TO JUNCTION PLANE  
ENTRY RAYS ARE  
PARALLEL TO THE  
OPTICAL AXIS (Z-AXIS)



Z-AXIS DIRECTION COSINE  
OF EXIT RAY

-0.999985  
-0.999990  
W7  
-0.999995  
-1.000000

0.0 0.2 0.4 0.6 [INCH]  
X0

ENTRY RAY DISTANCE FROM OPTICAL AXIS

+

+

THE OPTICAL AXIS  
IS NORMAL TO THE  
JUNCTION PLANE

+

+

+

ENTRY RAYS ARE  
PARALLEL TO THE  
OPTICAL AXIS  
(Z-AXIS)



13 surfaces BALLIRIS.OPT March 19, 1996 Normal incidence, at 0 degrees.

Index	Zvert	Xvert	Curvature	Mir/Lens	Dia.	Pitch	Notes
1.00029	-1.969	:	0.0	:	:	:	#1 vertex
1.00029	-1.969	:	0.507872	Lens	3.938	:	#2 B1, in
1.511186	-0.059	0.0	0.0	iris	0.906	-00.0	#3 stop 1
1.511186	0.000	:	0.0	iris	0.906	-00.0	#4 stop2
1.511186	0.059	-0.0	0.0	iris	0.906	-00.0	#5 stop 3
1.511186	3.799	:	-0.2632271	Mirror	7.598	:	#6 B2 mir.
1.511186	0.059	-0.0	0.0	iris	0.906	-00.0	#7 stop 3
1.511186	0.000	:	0.0	iris	0.906	-00.0	#8 stop 2
1.511186	-0.059	0.0	0.0	iris	0.906	-00.0	#9 stop 1
1.511186	-1.969	:	0.507872	Lens	3.938	:	#10 B1 out
1.00029	-1.969	:	0.0	:	:	:	#11 vertex
1.00029	-4724.4	:	0.0	iris	3.15	:	#12 lens
1.00029	-4724.41	:	0.0	:	:	:	#13 -120m

This file models the reflector's 0.118" stop thickness by using three thin irises.

17 rays RETBALL1.Z March 19, 1996

X0	Y0	Z0	U0	V0	W0	X4	X7	W7
0.05	0.0	-1.969	0.0	0.0	1.0	0.0331	-0.03258	-1.0000
0.15	0.0	-1.969	0.0	0.0	1.0	0.0993	-0.09776	-0.9996
0.25	0.0	-1.969	0.0	0.0	1.0	0.1656	-0.16304	-0.9990
0.35	0.0	-1.969	0.0	0.0	1.0	0.2321	-0.22849	-0.9981
0.45	0.0	-1.969	0.0	0.0	1.0	0.2988	-0.29415	-0.9969
0.55	0.0	-1.969	0.0	0.0	1.0	0.3658	-0.36009	-0.9955
0.60	0.0	-1.969	0.0	0.0	1.0	0.3994	-0.39317	-0.9947
0.668	0.0	-1.969	0.0	0.0	1.0	0.4453	-0.43830	-0.9935
0.6688	0.0	-1.969	0.0	0.0	1.0	0.4459	-0.43883	-0.9935
0.6689	0.0	-1.969	0.0	0.0	1.0	:	:	:
0.669	0.0	-1.969	0.0	0.0	1.0	:	:	:
0.677	0.0	-1.969	0.0	0.0	1.0	:	:	:
0.6775	0.0	-1.969	0.0	0.0	1.0	:	:	:
0.6777	0.0	-1.969	0.0	0.0	1.0	:	:	:
0.678	0.0	-1.969	0.0	0.0	1.0	:	:	:
0.679	0.0	-1.969	0.0	0.0	1.0	:	:	:
0.680	0.0	-1.969	0.0	0.0	1.0	:	:	:

The last seven rays are stopped. The finite 0.118" stop width has decreased the entrance pupil radius from 0.6775" to 0.6688".

surfaces BALLIRIS.OPT March 19, 1996 Oblique incidence at "I" degrees.

Index	Zvert	Xvert	Curvature	Mir/Lens	Dia.	Pitch	Notes
1.00029	-1.969	:	0.0	:refplane:	:	:	#1 vertex
1.00029	-1.969	:	0.507872	:Lens	: 3.938:	:	#2 B1, in
1.511186	-0.0295	0.051	0.0	:iris	: 0.906:-60.0:	:	#3 stop 1
1.511186	0.000	:	0.0	:iris	: 0.906:-60.0:	:	#4 stop2
1.511186	0.0295	-0.051	0.0	:iris	: 0.906:-60.0:	:	#5 stop 3
1.511186	3.799	:	-0.2632271	:Mirror	: 7.598:	:	#6 B2 mirror
1.511186	0.0295	-0.051	0.0	:iris	: 0.906:-60.0:	:	#7 stop 3
1.511186	0.000	:	0.0	:iris	: 0.906:-60.0:	:	#8 stop 2
1.511186	-0.0295	0.051	0.0	:iris	: 0.906:-60.0:	:	#9 stop 1
1.511186	-1.969	:	0.507872	:Lens	: 3.938:	:	#10 B1 out
1.00029	-1.969	:	0.0	:refplane:	:	:	#11 vertex
1.00029	-7874.01	:	0.0	:iris	: 3.15 :	:	#12 lens stop
1.00029	-7874.02	:	0.0	:refplane:	:	:	#13 lens plane
[Entry	:	:	:	:	:	:[-I ]:	:
Medium]	[Inch]	:[Inch]	[1/Inch]	:	:[Inch]	:[Deg]:	:

This file contains optical surface data used for a (BEAM THREE code) ray trace simulation of the University of Arizona ball retroreflectors manufactured for the NRAO Green Bank Telescope. The glass index used is the phase index for BK7 glass, at 0.78um wavelength. The ratio of the ball radii is 3.799"/1.969" = 1.929406.

Ray tracing for the case of a collimated ray bundle entering the ball at an angle I to the junction plane's normal direction is done as follows. One performs the ray trace for a parallel bundle at I = 0 degrees but tilts the retroreflector's aperture stops by -I. When a stop is not at the center of curvature of the balls, the stop center also requires a translation.

The file simulates the retroreflector taking into account the junction plane stop's thickness and rim cylindricality by placing three congruent thin irises in the ingoing and outgoing beam paths. If w is the aperture stop's thickness, the additional irises are placed at:  $X_v = \pm(-w/2)*\sin(I)$ ,  $Y_v = 0$ ,  $Z_v = \pm(w/2)*\cos(I)$ , and are tilted by (-I). Here  $w/2 = 0.059$  inches.

As a simplification, the stop diameter at ball 1 has not been reduced from the ball diameter to the ball's rim boundary diameter.

This file is used together with a file RETBALLQ.RAY, listing rays parallel to an arbitrary axis, which is the Z axis.

Ray spot patterns are generated at the ball's exit vertex plane and at 200 meters from the ball center. An 80mm diameter iris is placed just before the last surface, to simulate a laser scanner's detector lens rim stop.

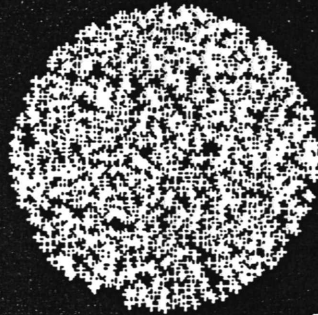
20 rays RETBALLQ.RAY March 19, 1996

X0	Y0	Z0	U0	V0	W0	X11	X13	Y13
0.20	0.0	-1.969	0.0	0.0	1.0	:	:	:
0.40	0.0	-1.969	0.0	0.0	1.0	:	:	:
0.4729	0.4729	-1.969	0.0	0.0	1.0	:	:	:
0.60	0.0	-1.969	0.0	0.0	1.0	:	:	:
0.6688	0.0	-1.969	0.0	0.0	1.0	:	:	:
0.00	0.20	-1.969	0.0	0.0	1.0	:	:	:
0.00	0.40	-1.969	0.0	0.0	1.0	:	:	:
-0.4729	0.4729	-1.969	0.0	0.0	1.0	:	:	:
0.00	0.60	-1.969	0.0	0.0	1.0	:	:	:
0.00	0.6688	-1.969	0.0	0.0	1.0	:	:	:
-0.20	0.0	-1.969	0.0	0.0	1.0	:	:	:
-0.40	0.0	-1.969	0.0	0.0	1.0	:	:	:
-0.4729	-0.4729	-1.969	0.0	0.0	1.0	:	:	:
-0.60	0.0	-1.969	0.0	0.0	1.0	:	:	:
-0.6688	0.0	-1.969	0.0	0.0	1.0	:	:	:
0.00	-0.20	-1.969	0.0	0.0	1.0	:	:	:
0.00	-0.40	-1.969	0.0	0.0	1.0	:	:	:
0.4729	-0.4729	-1.969	0.0	0.0	1.0	:	:	:
0.00	-0.60	-1.969	0.0	0.0	1.0	:	:	:
0.00	-0.6688	-1.969	0.0	0.0	1.0	:	:	:

GREEN BANK TELESCOPE BALL RETRO-REFLECTOR

EXIT RAY SPOT DISTRIBUTION IN PLANE TANGENT  
TO VERTEX POINT OF FIRST BALL SURFACE

1.0 [INCH]  
0.5  
X7  
0.0  
-0.5  
-1.0



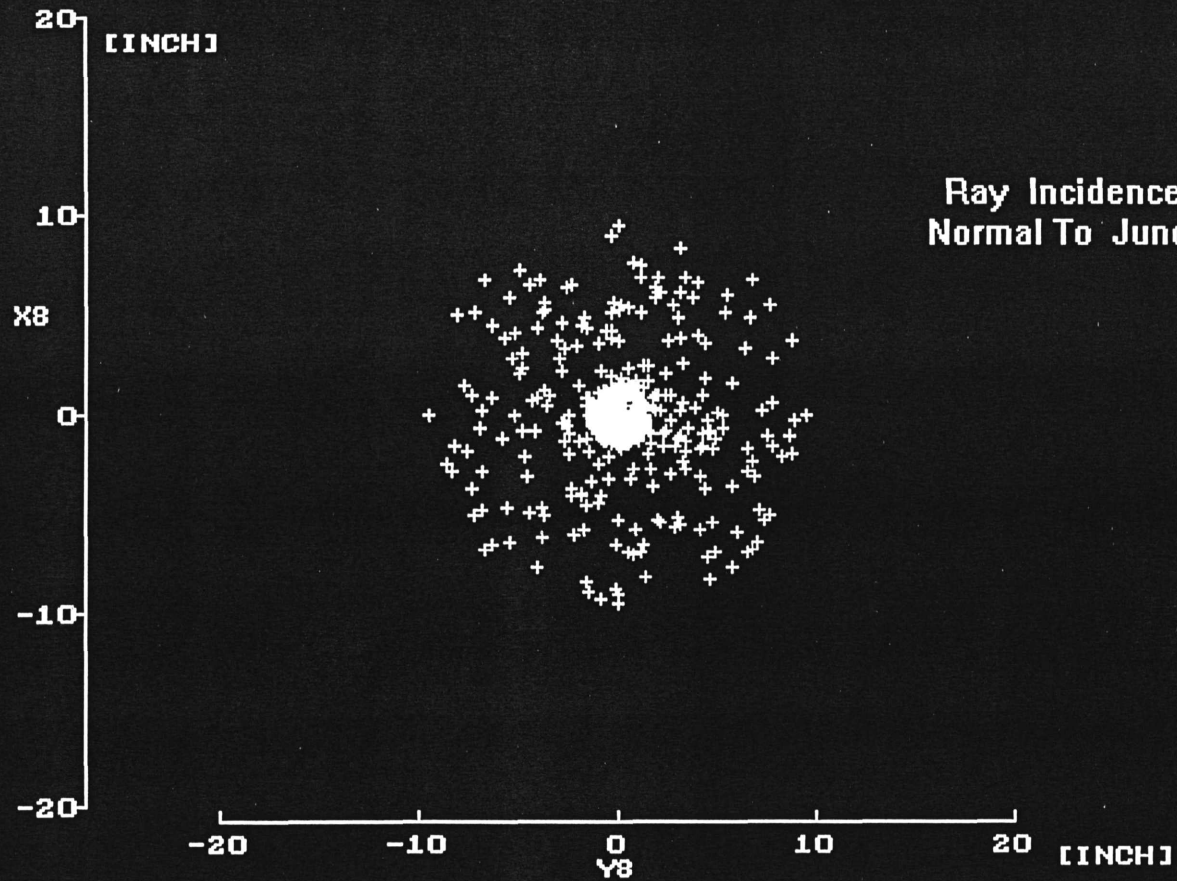
INPUT RAYS DISTRIBUTED  
UNIFORMLY OVER 1.358"  
SQUARE, IN THIS PLANE,  
CENTERED AT VERTEX POINT  
OF FIRST BALL SURFACE

AXIS-PARALLEL RAY ENTRY  
OPTIC AXIS AT 0 DEGREES  
TO JUNCTION PLANE NORMAL

-1.0 -0.5 0.0 0.5 1.0 [INCH]  
Y7

starts= 2408 finishes= 1893: 78.6%

Ray Return At 40 Meters Distance For Collimated  
Entry Ray Bundle 1.355" Square

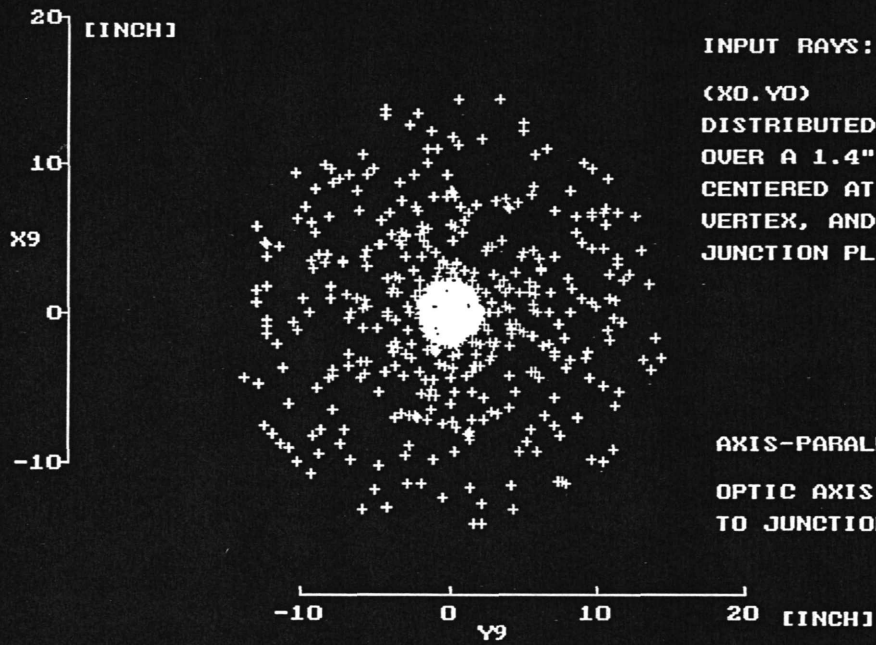


Ray Incidence Is  
Normal To Junction Plane

starts= 639 finishes= 504: 78.9%

# GREEN BANK TELESCOPE BALL RETROREFLECTOR

EXIT RAY SPOT TRACE AT 60 METERS FROM BALL CENTER



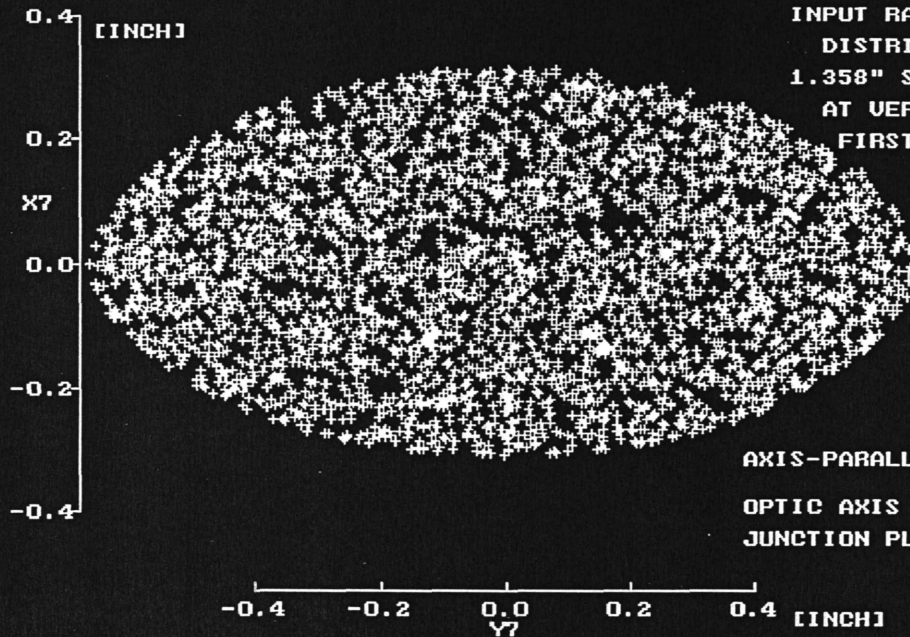
INPUT RAYS:

(X0, Y0)  
DISTRIBUTED UNIFORMLY  
OVER A 1.4" SQUARE,  
CENTERED AT FRONT BALL  
VERTEX, AND PARALLEL TO  
JUNCTION PLANE

AXIS-PARALLEL RAY ENTRY  
OPTIC AXIS AT 0 DEGREES  
TO JUNCTION PLANE NORMAL

starts= 1062 finishes= 799: 75.2%

EXIT RAY SPOT DISTRIBUTION IN PLANE TANGENT  
TO VERTEX POINT OF FIRST BALL SURFACE

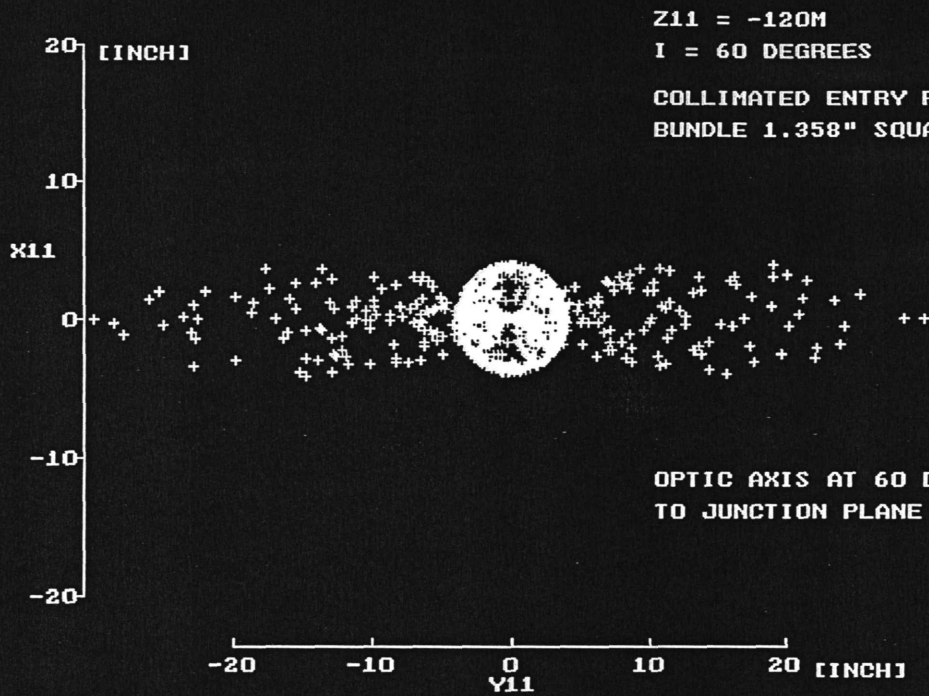


INPUT RAYS UNIFORMLY  
DISTRIBUTED OVER  
1.358" SQUARE CENTERED  
AT VERTEX POINT OF  
FIRST BALL SURFACE

AXIS-PARALLEL RAY ENTRY  
OPTIC AXIS 60 DEGREES TO  
JUNCTION PLANE NORMAL

starts= 10533 finishes= 3673: 34.9%





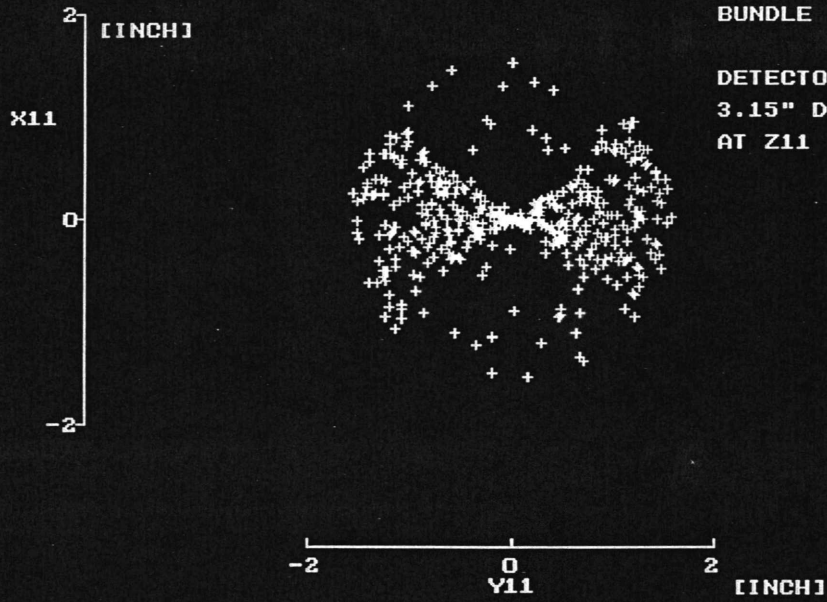
starts= 2813 finishes= 982: 34.9%

Z11 = -120M

I = 63 DEGREES

COLLIMATED ENTRY RAY  
BUNDLE 1.358" SQUARE

DETECTOR LENS RIM STOP  
3.15" DIAMETER PLACED  
AT Z11



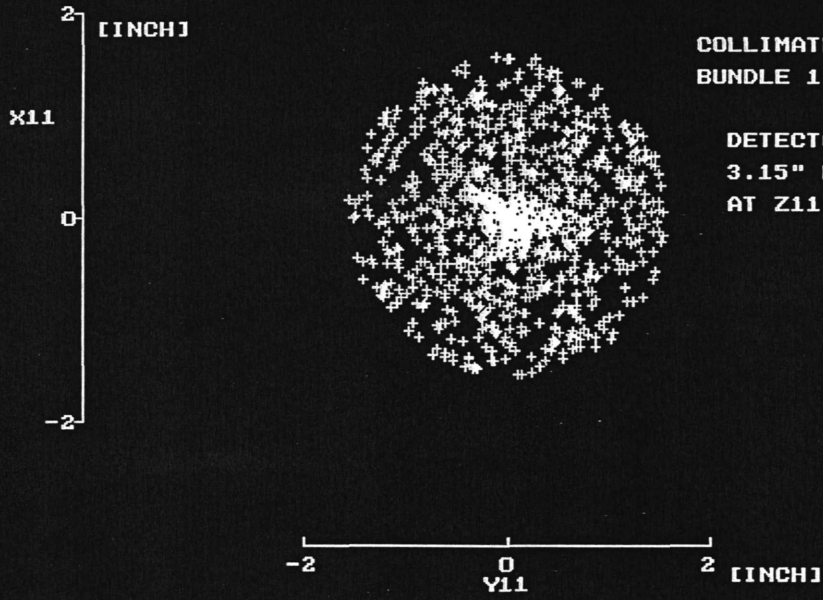
starts= 10847 finishes= 466: 4.3%

Z11 = -120M

I = 45 DEGREES

COLLIMATED ENTRY RAY  
BUNDLE 1.358" SQUARE

DETECTOR LENS RIM STOP  
3.15" DIAMETER PLACED  
AT Z11



starts= 10842 finishes= 1065: 9.8%

SPOT DIAGRAM OF  
RAYS ON TANGENT PLANE TO FIRST BALL VERTEX  
WHICH ARRIVE WITHIN 3.15" DIAMETER OF DETECTOR LENS  
AT 120 METERS DISTANCE FROM BALL CENTER

0.5  
[INCH]  
X7  
0.0  
-0.5

-0.5 0.0 0.5 [INCH]  
Y7

AXIS PARALLEL RAY ENTRY  
OPTIC AXIS 63 DEGREES TO  
JUNCTION PLANE NORMAL

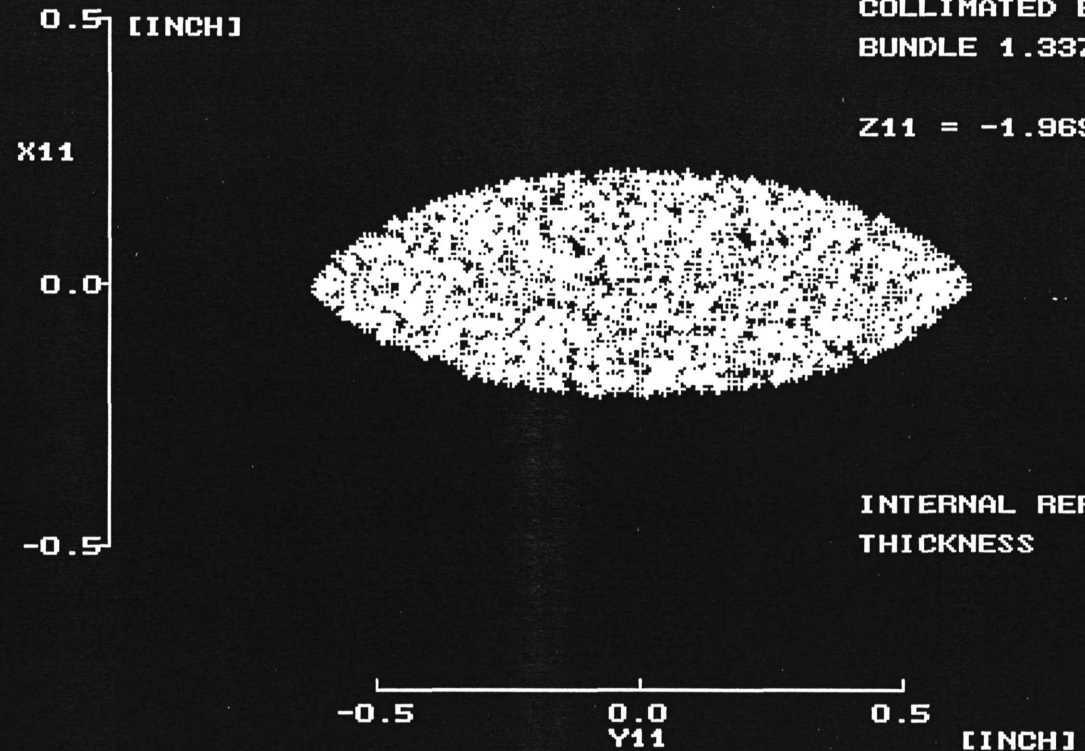
starts= 11000 finishes= 486: 4.4%

SPOT DIAGRAM OF EMERGENT RAYS FROM BALL RETROREFLECTOR  
AT VERTEX TANGENT PLANE TO FIRST BALL SURFACE

I = 63 DEGREES

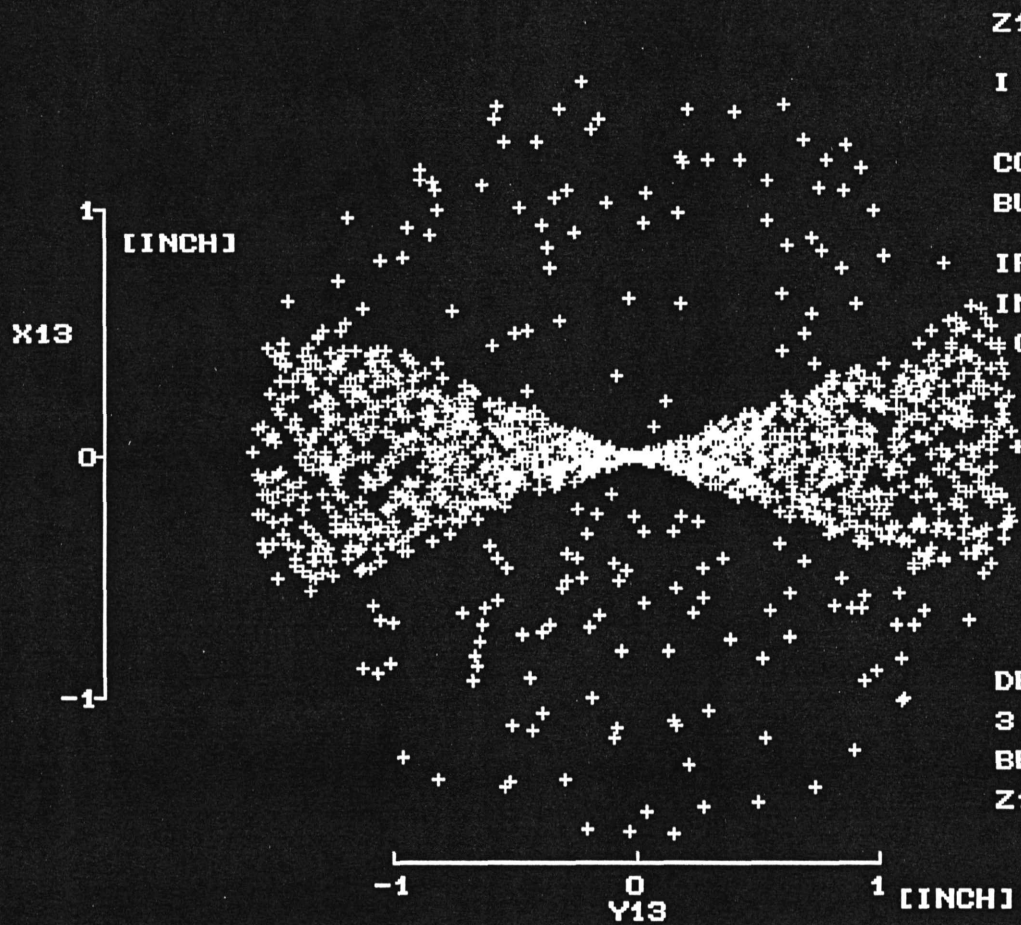
COLLIMATED ENTRY RAY  
BUNDLE 1.3376" SQUARE

Z11 = -1.969M



INTERNAL REFLECTOR STOP  
THICKNESS 0.118"

starts= 15278 finishes= 3307: 21.6%



Z13 = -200M

I = 63 DEGREES

COLLIMATED ENTRY RAY  
BUNDLE 1.3376" SQUARE

IRIS STOP THICKNESS  
INSIDE REFLECTOR IS  
0.118"

DETECTOR LENS RIM STOP  
3.15" DIAMETER PLACED  
BEFORE THE PLANE  
Z13 = -200M

starts= 90890 finishes= 1399: 1.5%